# Hydrodynamic boundary effects on thermophoresis of confined colloids

Aloïs Würger

# Hydrodynamic boundary effects on thermophoresis of confined colloids

Alois Würger
*Laboratoire Ondes et Matière d'Aquitaine, Université de Bordeaux & CNRS, 33405 Talence, France*

We study hydrodynamic slowing-down of a particle moving in a temperature gradient perpendicular to a wall. At distances much smaller than the particle radius, $h \ll a$, lubrication approximation leads to the reduced velocity $u/u_0 = 3\frac{h}{a}(\ln\frac{a}{h} - \frac{9}{4})$, where $u_0$ is the velocity in the bulk. With Brenner's result for confined diffusion, we find that the trapping efficiency, or effective Soret coefficient, increases logarithmically as the particle gets very close to the wall. Our results provide a quantitative explanation for the recently observed enhancement of thermophoretic trapping at short distances. Our discussion of parallel and perpendicular thermophoresis in a capillary, reveals a good agreement with experiments on charged polystyrene particles, and sheds some light on a controversy concerning the size-dependence and the non-equilibrium nature of the Soret effect.

PACS numbers:

The motion of a colloid close to a solid boundary is strongly influenced by hydrodynamic interactions. Thus the like-charge attractions observed for confined colloidal assemblies [1], were shown to arise from hydrodynamic fluctuations [2]. Similarly, a driven particle close to a wall induces a lateral flow field which favors cluster formation [3–7]. More recently, the collision patterns observed for self-propelling Janus particles [8], were related to hydrodynamic coupling to the wall [9, 10]. Quite generally, the latter are relevant where surface forces and confined geometries are combined for sieving [11], trapping [12, 13], and assembling colloidal beads [14].

A generic example is provided by a particle moving towards a wall due to surface forces. If hydrodynamic effects on Brownian motion are well understood in terms of Brenner's solution for confined diffusion [15], this is not the case for the drift velocity $u$. Previous studies on confined electrophoresis, diffusiophoresis, and pairs of self-propelling spheres, indicate a slowing-down due to hydrodynamic coupling [16–19]; yet so far there is no satisfactory solution for the lubrication regime $h < a$.

Electric fields and chemical gradients are strongly altered by the wall-solvent-particle permittivity or diffusivity contrast; experimentally, this coupling is difficult to separate from hydrodynamic interactions. A more favorable situation occurs for thermophoresis, where the drift velocity is proportional to the temperature gradient [20, 21]: Since the heat conductivity of silica or polystyrene (PS) particles is not very different from that of water, the thermal gradient is hardly affected by the presence of the wall [7], and velocity changes can be unambiguously attributed to hydrodynamic interactions.

Here we study the vertical motion of a particle that is confined to the upper half-space $z \geq 0$, as illustrated in Fig. 1. We consider thermophoretic driving, $u = D_T\nabla T$, with mobility coefficient $D_T$; yet most of the paper applies equally well to other mechanisms. In the steady state, drift and diffusion currents cancel each other, $-uc - D\nabla c = 0$, and the particle concentration satisfies

$$-\nabla \ln c = \frac{u}{D}, \qquad (1)$$

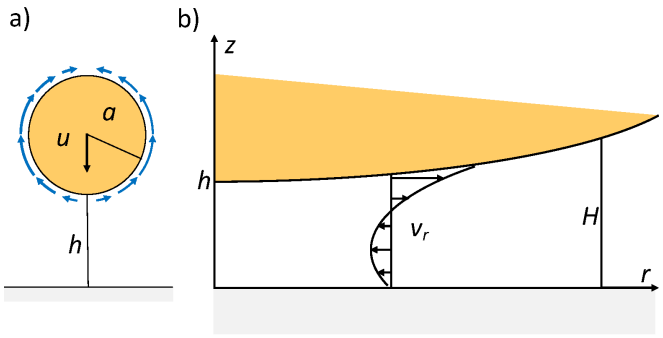


FIG. 1: Schematic view of a particle moving towards a confining wall at velocity $u$. a) The arrows along the particle surface indicate the slip velocity $v_s$ induced by thermodynamic forces. b) In the narrow slit of width $H(r) = h + a - \sqrt{a^2 - r^2}$, the vertical particle motion and the outward slip velocity result in an intricate radial flow profile $v_r$.

where the gradient is along the vertical direction and $c$ is a function of $h$. At large distances $h \gg a$, there are no boundary effects and Eq. (1) is readily integrated, $c = c_0 e^{-h/\ell_0}$, with the trapping length $\ell_0 = D_0/u_0$ [22]. As the particle approaches the wall, both drift and diffusion are slowed down by hydrodynamic coupling. For thermophoretic trapping, this is best expressed in terms of the Soret coefficient $S_T = D_T/D$ which is related to (1) through $u/D = S_T\nabla T$.

The present work was partly motivated by the recent observation that thermophoretic trapping at very short distances is much stronger than in the bulk [23]. The main objectives are to evaluate the drift velocity $u$ in the lubrication regime, and to discuss available Soret data in view of hydrodynamic effects. Comparing our results with six independent experiments, sheds some light on a controversy whether or not the Soret coefficient can be obtained from the equilibrium Gibbs energy [24].

*Hydrodynamic boundary effects.* Thermophoresis arises from the thermal non-equlibrium properties of the boundary layer close to the particle. The component of the temperature gradient parallel to the particle sur-

face, induces an effective slip velocity $v_s \propto \nabla_{||} T$ [21, 25]. Throughout this paper we neglect the thickness of the interaction layer and thus treat $v_s$ as a boundary condition for the velocity field in the surrounding fluid [25]. With the notation of Fig. 1 one has $v_s = \frac{3}{2} u_0 (r/a)$, where $u_0$ is the thermophoretic velocity of a particle in the bulk, and $r$ the radial distance from the vertical axis.

As the particle approaches the boundary, the wall squeezes the flow field and thus reduces the drift velocity to the value $u$. At very short distances, as shown in Fig. 1b, the flow in the slit is well described by lubrication approximation, with the radial velocity field

$$v_r(z) = v_s \left( \frac{z}{H} - \frac{3z(H-z)}{H^2} \right) + 3u \frac{r}{H} \frac{z(H-z)}{H^2}. \quad (2)$$

The first term accounts for the slip velocity $v_s$, and satisfies the conditions $v_r|_0 = 0$ at the solid boundary and $v_r|_H = v_s$ at the particle surface $H$. Integrating over $z$, one finds that its net flow vanishes. The second term arises from the particle velocity $u$; one readily verifies that the vertical volume flow $\pi r^2 u$ within a radius $r$, is cancelled by the radial flow through a cylinder of radius $r$ and height $H$, that is, the $z$-integral of $2\pi r v_r$.

The relation between the particle velocity $u$ and its bulk value $u_0$, is established by noting that there is no force $F$ acting on the particle. From the radial component of Stokes' equation, $\partial_r P = \eta \partial_z^2 v_r$, we obtain the pressure gradient $\partial_r P = 6\eta v_s / H^2 - 6\eta u r / H^3$ which, upon integration, gives $P(r)$. Since the diagonal component of the viscous stress vanishes, $\sigma_{zz} = 0$, the force is given by the surface integral along the wall,

$$F = \int dS P(r, z=0) \stackrel{!}{=} 0. \quad (3)$$

The second equality expresses the fact that there is no mechanical or 'thermophoretic' force acting on the particle. In evaluating $P$ and $F$, we use the width $H = h + a - \sqrt{a^2 - r^2}$, instead of the common approximation $H = h + r^2/2a$ [26]. Thus we avoid the problem of how to match the pressure to its bulk value [18].

The condition (3) provides a relation between $u$ and $u_0$, and thus quantifies the hydrodynamic effects on the drift velocity,

$$\frac{u}{u_0} = \frac{h}{a} \phi(h/a) \qquad (h \ll a), \quad (4)$$

with

$$\phi(\hat{h}) = 3(1+\hat{h}) \frac{(2 + 6\hat{h} + 3\hat{h}^2) \ln \frac{\hat{h}+1}{\hat{h}} - \frac{3}{2}(3 + 2\hat{h})}{2 + 9\hat{h} + 6\hat{h}^2 - 6\hat{h}(1+\hat{h})^2 \ln \frac{\hat{h}+1}{\hat{h}}} \quad (5)$$

and the shorthand notation $\hat{h} = h/a$. At very small distances it simplifies to

$$\phi = -3(\ln \hat{h} + 9/4); \quad (6)$$

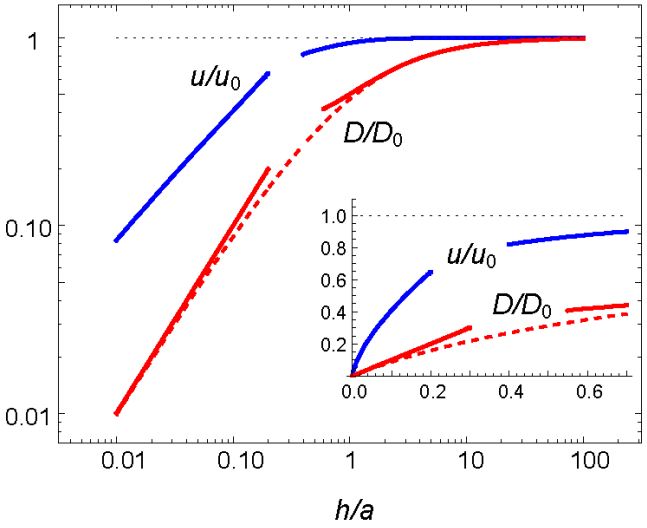


FIG. 2: Reduced drift velocity $u/u_0$ and diffusion coefficient $D/D_0$ for a particle moving toward a wall, as a function of the relative distance $\hat{h} = h/R$. The curves at small $\hat{h}$ are given by (4) and (8), those at large $\hat{h}$ by (7) and (9). The dashed line is calculated from Brenner's exact series for $D/D_0$ [15]. At all distances, the diffusion coefficient is more strongly reduced than the drift velocity. The inset shows the same at linear scale, thus highlighting the linear law $D \propto \hat{h}$ and the logarithmic corrections for $u$ at short distances

the full expression (5) is required in the experimentally relevant range $\hat{h} \geq 0.01$, which is set by the presence of electric-double layer and dispersion forces [23].

Now we turn to the case where the distance exceeds the particle size, $h > a$. Following Keh and Anderson [16], we start from the velocity field in a bulk liquid and evaluate the first reflection at the wall [26]. The resulting correction to the particle velocity vanishes as $h^{-3}$,

$$\frac{u}{u_0} = 1 - \frac{1}{2} \frac{a^3}{(h+a)^3} \qquad (h > a). \quad (7)$$

A slightly larger correction, with a prefactor $\frac{5}{8}$ instead of $\frac{1}{2}$, was found for the electrophoretic mobility [16]. The difference of $\frac{1}{8}$ arises from the deformation of the electric field by the low-permittivity particle and by the conducting wall. In the case of thermophoresis, the corresponding effect on the local temperature gradient is small, because of the relatively weak thermal conductivity contrast at the particle-solvent-wall interfaces [26]. A more complex situation occurs if ion currents are relevant for the slip velocity, e.g., through the Seebeck effect [22, 27] or a permittivity change due to phase separation [28, 29].

Fig. 2 shows the reduced velocity $u/u_0$ as a function of distance; it changes rather little for $h > a$, but drops to zero as $h \to 0$. For comparison we also plot the corresponding expressions $D/D_0$ for the diffusion coefficient. At small distances, the lubrication approximation results in the well-known linear variation with $h$,

$$D/D_0 = h/a \qquad (h < a), \quad (8)$$

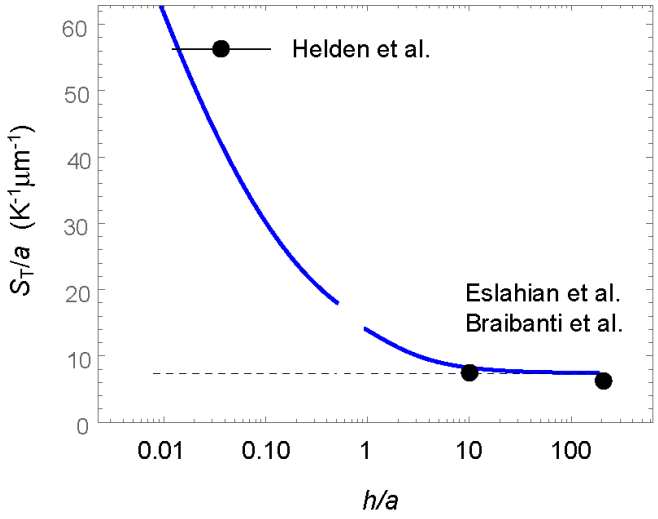


FIG. 3: Hydrodynamic effects on the effective Soret coefficient $S_T/a$. The solid lines show the results from lubrication approximation (10) and the method of reflection from (11); the dashed line gives the bulk value $S_T^0/a = 7.4$ K$^{-1}\mu$m$^{-1}$ [26]. The experimental points are from Table I.

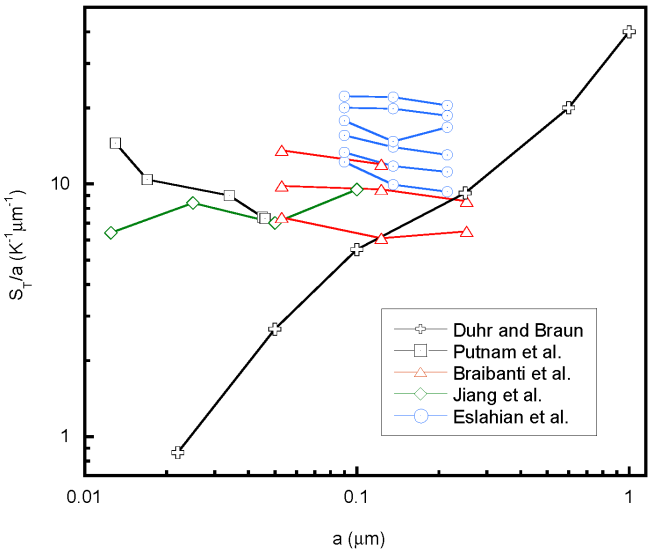


FIG. 4: Size dependence of the Soret coefficient $S_T$. For the data of five experiments on polystryene particles, the ratio of $S_T$ and the particle radius $a$ is plotted as a function of $a$. The data (+) are taken at room temperature, Duhr and Braun [37]; (□) above 35 °C, Putnam et al. [34]; (△) at 25, 35, 45 °C, Braibanti et al. [35]; (◇) Jiang et al. [36]; (◯) at 28, 31, 35, 39, 44, 47 °C, Eslahian et al. [22]. The lines connect data at constant temperature. Details are given in [26].

whereas to third order in the inverse distance, the reflection method results in

$$\frac{D}{D_0} = 1 - \frac{9}{8}\frac{a}{h+a} + \frac{1}{2}\frac{a^3}{(h+a)^3} \qquad (h > a). \qquad (9)$$

These limiting laws are compared with Brenner's exact series for the diffusion coefficient of a confined particle [15], which is given by the dashed line. As a general rule, hydrodynamic slowing down is significantly stronger for diffusion, as a consequence of the long-range velocity field accompanying Browian motion.

*Thermophoretic trapping.* In view of a recent Soret experiment by Helden et al. [23], we discuss confined thermophoresis, where the stationary distribution (1) defines the Soret coefficient $S_T$ through $u/D = S_T\nabla T$. In a 1D geometry with constant temperature gradient, one obtains hydrodynamic effects as the ratio of the correction factors for drift and diffusion. In lubrication approximation, this results in

$$S_T = S_T^0\phi(\hat{h}) \qquad (\hat{h} < 1), \qquad (10)$$

whereas in the opposite limit we have

$$S_T = S_T^0\frac{1 - \frac{1}{2}\frac{1}{(1+\hat{h})^3}}{1 - \frac{9}{8}\frac{1}{1+\hat{h}} + \frac{1}{2}\frac{1}{(1+\hat{h})^3}} \qquad (\hat{h} > 1). \qquad (11)$$

In Fig. 3 we plot the Soret coefficient as a function of the reduced distance $h/a$. As the particle gets closer to the wall, trapping is enhanced by hydrodynamic interactions, the Soret coefficient increases with respect to the bulk value, and at $\hat{h} \to 0$ diverges logarithmically.

The bulk Soret coefficient.varies linearly with the particle radius, $S_T^0 \propto a$, due to the inverse variation of the Stokes-Einstein coefficient $D_0 = k_BT/(6\pi\eta a)$ [30] and the constant drift velocity $u_0$ [25]. In order to facilitate the comparison of Soret data for particles of different radius, we plot the ratio $S_T/a$. Our findings provide a quantitative explanation for the data of Helden et al. [23]: For polystyrene particles ($a = 2.5\mu$m) very close to a wall ($h < 0.3\mu$m), these authors reported $S_T = 140$ K$^{-1}$ at room temperature; the reduced value $S_T/a$ is about eight times larger than those reported in previous experiments on particles at large distances; see Fig. 3 and Table I. The quantitative agreement with the present theory provides evidence that the enhanced trapping is of hydrodynamic origin. This is corroborated by the sim-

TABLE I: Soret data for polystyrene particles in capillaries with a perpendicular temperature gradient [22, 23, 35]. The numbers $S_T/a$ give the data shown in Fig. 5 [35], or their extrapolation to $T = 25°$ [22]; that of Helden et al. is taken from Fig. 4 of [23]. The values for the distance $h$ correspond to the range where data are taken [23] or, for weak trapping, to $\ell_0 = D_0/u_0$ [22, 35]; the value for Ref. [35] indicates a lower bound. For a more detailed analysis, see [26].

| $T = 25°$ C | $S_T/a$ (K$^{-1}\mu$m$^{-1}$) | $h$ ($\mu$m) | $h/a$ |
|---|---|---|---|
| Helden et al. [23] | 56 | 0.03 – 0.3 | 0.012 – 0.12 |
| Eslahian et al. [22] | 7.4 | 2 | 9 |
| Braibanti et al. [35] | 6.5 | > 50 | > 200 |

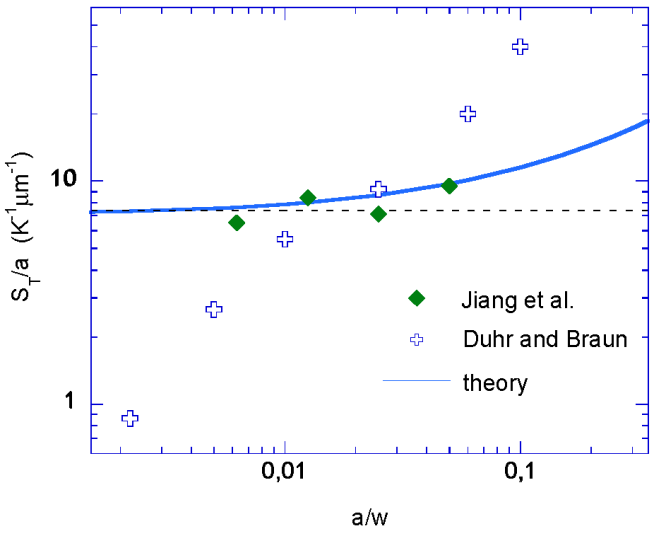


FIG. 5: Thermophoretic trapping parallel to the capillary. We show $S_T/a$ as a function of $a/w$. The data of Duhr and Braun are taken in a capillary of width $w = 10\mu$m [37], and those of Jiang et al. in $w = 2\mu$m [36]. The solid line is calculated from (12) where hydrodynamic effects are accounted for by Oseen's model for the parallel diffusion coefficient. The dashed line indicates the bulk value $S_T^0/a = 7.4$ K$^{-1}\mu$m$^{-1}$.

ilar temperature series observed at small [23] and large distances [22, 35].

Since the linear size dependence of $S_T^0$ is essential for the above argument, we recall its theoretical foundation and experimental confirmation. If the Stokes-Einstein coefficient needs no further discussion, a few words are in order concerning $u_0$. As first shown by von Smoluchowski in his study of thin-boundary layer electrophoresis [31], the equilibrium between surface forces and viscous stress is independent of the particle radius, and so is the velocity $u_0$. Later on, Derjaguin generalized this argument to motion driven by composition and temperature gradients [32]. The law $u_0 =$const. ceases to be valid for boundary conditions with large Navier slip length [33] and for particles smaller than the Debye length [21]; yet none of these cases is relevant for the systems considered here.

Fig. 4 shows $S_T/a$ as a function of $a$, measured for PS particles in five experiments. In the setup of Refs. [22, 34, 35] the temperature gradient is perpendicular to the boundary as in Fig. 1; a parallel configuration is used in [36, 37], with the particles moving along the capillary. The data of [22, 34–36] show the behavior $S_T/a =$ const. expected for large $h$, and even their absolute values agree well with each other. A constant ratio was also observed for surfacted microemulsion droplets [38]. On the contrary, Duhr and Braun reported a linear variation $S_T/a \propto a$ over two orders of magnitude [37].

*Motion parallel to the capillary.* In view of this discrepancy we complete our discussion of hydrodynamic effects by considering thermophoresis along the boundaries. The degree of confinement, as given by the ratio of the particle radius $a$ and the width $w$ of the capillary, is small in the setup of Refs. [36, 37]. Thus we treat the perturbative range $a \ll w$ only. In Oseen's model for parallel diffusion, confinement reduces the Stokes-Einstein coefficient of a particle at vertical position $z$ according to $D_0/D_\parallel = 1 + \frac{9}{8}\frac{a}{z} + \frac{9}{8}\frac{a}{w-z}$ [15]. The thermophoretic velocity is hardly affected by the walls, in leading order we have $u/u_0 = 1$; a more complex behavior occurs close to the wall [39]. Taking the position average in the interval $[a, w-a]$, we find

$$\frac{S_T}{S_T^0} = 1 + \frac{9}{4}\frac{a}{(w-2a)}\ln\frac{w-a}{a} \qquad (a \ll w). \tag{12}$$

In Fig. 5 we plot the Soret data of Refs. [36, 37] as a function of $a/w$, and compare with the theoretical expression (12). If the four data points of Jiang et al. [36] agree with theory, this is not the case for those of Duhr and Braun: The Soret effect of the biggest particles ($a = 1$ $\mu$m) is three times stronger, whereas that of the smallest one ($a = 22$ nm) is by one order of magnitude too weak. This discrepancy can not be explained by higher-order terms in (12) or by additional effects such as thermoosmosis along the capillary.

Summarizing the preceding discussion, we find a quantitative agreement with the experiments of Refs. [22, 23, 34–36]: As illustrated in Figs. 3, 4 and 5, the Soret data show the expected linear size dependence, agree on the bulk value $S_T^0/a = 7.4$ K$^{-1}\mu$m$^{-1}$, and confirm the hydrodynamic boundary effects obtained in this work. The discrepancy of the data of Duhr and Braun [37] is probably of some other, so far unknown origin [35]. This evidence sheds some doubt on the model of Ref. [37], which was coined to describe the size dependence $S_T \propto a^2$ and was recently applied to DNA [40]. In this model, the Soret coefficient is given by a derivative of the particle's Gibbs energy, $S_T = (k_BT)^{-1}dG/dT$, whereas the hydrodynamic approach results in dissipative factors that cannot be derived from equilibrium thermodynamics [24].

*Conclusion.* We have studied hydrodynamic effects on colloidal particles approaching a wall. In the lubrication regime, the analytical solution (5) shows the expected logarithmic behavior at very small distance, but describes also the experimentally relevant range $\hat{h} \sim \frac{1}{10}$. Our theory provides a quantitative explanation for the recently observed enhancement of confined thermophoresis [23]. Comparison of available data partly elucidates a controversy on the size dependence of thermophoresis, and confirms Derjaguin's approach based on surface forces and hydrodynamics.

Stimulating discussions with L. Helden are gratefully acknowledged. This work was supported by Agence Nationale de la Recherche through contract ANR-13-IS04-0003.

[1] A.E. Larsen, D. G. Grier, Nature **385**, 230 (1997)
[2] T.M. Squires, M.P. Brenner, Phys. Rev. Lett. **85**, 4976 (2000)
[3] M. Trau, D. Saville, and A. I. Askay, Science **272**, 706 (1996)
[4] S.R. Yeh, M. Seul, B.I. Shraiman, Nature **386**, 57 (1997)
[5] F.M. Weinert, D. Braun, Phys. Rev. Lett. **101**, 168301 (2008)
[6] R. Di Leonardo, F. Ianni, G. Ruocco, Langmuir **25**, 4247 (2009)
[7] J. Morthomas, A. Würger, Phys. Rev. E **81**, 051405 (2010)
[8] G. Volpe, I. Buttinoni, D. Vogt, H.-J. Kümmerer, and C. Bechinger, Soft Matter **7**, 8810 (2011)
[9] S.E. Spagnolie and E. Lauga, J. Fluid Mech. **700**, 105.(2012)
[10] K. Schaar, A. Zöttl, H. Stark, Phys. Rev. Lett. **115**, 038101 (2015)
[11] A. Cuche, A. Canaguier-Durand, E. Devaux, J. A. Hutchison, C. Genet, T.W. Ebbesen, Nano Lett. **13**, 4230 (2013)
[12] J. Chen, Z. Kang, S.K. Kong, and H.-P. Ho, Optics Lett. **40**, 3926 (2015)
[13] M. Braun, A. Würger and F. Cichos, Phys. Chem. Chem. Phys. **16**, 15207 (2014)
[14] I. Theurkauff, C. Cottin-Bizonne, J. Palacci, C. Ybert, L. Bocquet, Phys. Rev. Lett. **108**, 268303 (2012)
[15] H. Brenner, Chem. Eng. Sci. **16**, 242 (1961)
[16] H.J. Keh, J.L. Anderson, J. Fluid Mech. **153**, 417 (1985)
[17] M. Loewenberg and R.H. Davis, J. Fluid Mech. **288**, 103.(1995)
[18] T. Ishikawa, M.P. Simmonds, T.J. Pedley J. Fluid Mech. **568**, 119 (2004)
[19] Y.C. Chang, H.J. Keh, J. Colloid Interf. Sci. **322**, 634 (2008)
[20] R. Piazza, Soft Matter **4**, 1740 (2008).
[21] A. Würger, Rep. Prog. Phys. **73**, 126601 (2010)
[22] K.A. Eslahian, A. Majee, M. Maskos, A. Würger, Soft Matter **10**, 1931 (2014)
[23] L. Helden, R. Eichhorn, C. Bechinger, Soft Matter **11**, 2379 (2015)
[24] A. Würger, C. R. Mecanique **341**, 438 (2013)
[25] J.L. Anderson, Ann. Rev. Fluid Mech. **21**, 61 (1989)
[26] See Supplemental material for technical details
[27] A. Würger, Phys. Rev. Lett. **101**, 108302 (2008)
[28] I. Buttinoni, G. Volpe, F. Kümmel, G. Volpe, and C. Bechinger, J. Phys. Condens. Matter **24**, 284129 (2012)
[29] A. Würger, Phys. Rev. Lett. **115**, 188304 (2015)
[30] A. Einstein, Annal. Phys. **19**, 371 (1906)
[31] M. von Smoluchowski, Bull. Int. Acad. Sci. Cracovie **184**.(1903)
[32] N.V. Churaev, B.V. Derjaguin, V.M. Muller, *Surface Forces*, Plenum Publishing Corporation (New York 1987)
[33] J. Morthomas, A. Würger, J. Phys. Condens. Matt. **21**, 035103 (2009)
[34] S.A. Putnam, D.G. Cahill, G.C.L. Wong, Langmuir **23**, 9221 (2007)
[35] M. Braibanti, D. Vigolo, R. Piazza, Phys. Rev. Lett. **100**, 108303 (2008).
[36] H.-R. Jiang, H. Wada, N. Yoshinaga and M. Sano, Phys. Rev. Lett. **102**, 208301 (2009)
[37] S. Duhr, D. Braun, Phys. Rev. Lett. **96**, 168301 (2006)
[38] D. Vigolo, G. Brambilla, R. Piazza, Phys. Rev. E **75**, 040401 (2007)
[39] E. Yariv and H. Brenner, J. Fluid Mech. **484**, 85.(2003)
[40] M. Reichl, M. Herzog, A. Götz, and D. Braun, Phys. Rev. Lett. **112**, 198101 (2014)

# Hydrodynamic boundary effects on thermophoresis of confined colloids - Supplemental material

Alois Würger
*Laboratoire Ondes et Matière d'Aquitaine, Université de Bordeaux & CNRS, 33405 Talence, France*

PACS numbers:

Here we study hydrodynamic effects on a colloidal particle moving towards a solid wall. The corresponding current reads as

$$J = -uc - D\nabla c, \tag{1}$$

where $D$ the Stokes-Einstein coefficient and $u$ is the drift velocity. In the steady state $J = 0$, drift and diffusion currents cancel each other, and the particle concentration satisfies

$$-\nabla \ln c = \frac{u}{D} = \frac{1}{\ell}. \tag{2}$$

We assume $u > 0$, such that the particle is trapped close to the solid wall and the trapping length $\ell = D/u$ results from Brownian motion vs. uniform drift.

The velocity field in the surrounding fluid satisfies Stokes' equation

$$\eta \boldsymbol{\nabla}^2 \mathbf{v} = \boldsymbol{\nabla} P \tag{3}$$

and the incompressibility condition $\boldsymbol{\nabla}\cdot\mathbf{v} = 0$, with appropriate boundary conditions on the particle surface and on the confining wall. The thermal forces induce an effective slip on the particle

$$v_s = v_0 \sin\theta, \tag{4}$$

where $\theta$ is the angle between the surface normal and the applied gradient. The prefactor is related to the particle velocity in a bulk fluid, $v_0 = \frac{3}{2}u_0$. (Our sign convention relates an upward slip velocity, like in Fig. 1, to a downward particle motion.)

If the trapping length is much larger than the particle size, $\ell \gg a$, boundary effects are of little relevance, and the trapping length can be evaluated with the bulk velocity and diffusion coefficient, $1/\ell_0 = u_0/D_0$. Then the probability distribution function is readily integrated,

$$c(h) = c_0 e^{-(a+h)/\ell_0}, \qquad (h \gg a), \tag{5}$$

where $a+h$ is the vertical coordinate of the particle center. At large distances, hydrodynamic effects are evaluated with the method of reflections; they result in small corrections to the trapping length, which are given in powers of $a/(a+h)$.

This paper deals mainly with particles close to the boundary, $h \ll a$, where hydrodynamic effects are strong and where the lubrication approximation is the appropriate appraoch.

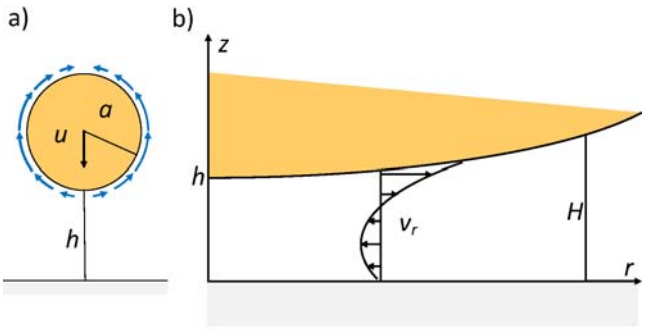


FIG. 1: Schematic view of a particle moving towards a confining wall at velocity $u$. a) The arrows along the particle surface indicate the slip velocity $v_s$ induced by thermodynamic forces. b) In the narrow slit of width $H(r) = h + a - \sqrt{a^2 - r^2}$, the vertical particle motion and the outward slip velocity result in an intricate radial flow profile $v_r$.

## I. LUBRICATION APPROXIMATION

Stokes' equation simplifies significantly in a narrow slit with slowly varying boundary conditions on the confining surfaces. Then the radial derivatives are much smaller than those with respect to the vertical coordinate $z$, and the vertical velocity component is small as compared to the vertical one. In this case the radial component of (3) reads

$$\eta \partial_z^2 v_r = \partial_r P. \tag{6}$$

This simplified equation is valid for narrow slits and relies on the small parameter $h/a \ll 1$.

In lubrication approximation we assume a parabolic velocity profile, implying a constant pressure across the slit, $\partial_z P = 0$. Then the radial velocity reads

$$v_r = \frac{3}{2}u_0 \frac{r}{a}\left(\frac{z}{H} - \frac{3z(H-z)}{H^2}\right) + 3u\frac{r}{H}\frac{z(H-z)}{H^2}. \tag{7}$$

The first term arises from the slip velocity (4) along the particle surface, $v_s = \frac{3}{2}u_0 \sin\theta$ with $\sin\theta = r/a$, and the second one from the vertical motion of particle at the reduced velocity $u$. One readily verifies the conditions on the solid boundary, $v_r|_{z=0} = 0$, and on the particle surface, $v_r|_{z=h} = v_s$. The width of the slit is

$$H = h + a - \sqrt{a^2 - r^2};$$

in the following we do *not* use the truncated series $H_{\rm tr} = h + r^2/2a$.

The quadratic Poiseuille flow in parentheses assures that there is no net flow due to the slip velocity. On the other hand, the motion of the particle towards the wall at velocity $u$, results in a finite outward flux which increases with the radius $r$ according to

$$2\pi r \int_0^H dz v_r = \pi u r^2 H, \tag{8}$$

and thus is identical to the vertical incoming flux through the disc of radius $r$.

The related pressure is obtained from Stokes' equation (6),

$$\partial_r P = \eta \frac{9 r u_0}{2H^2 a} - \eta \frac{6ru}{H^3}. \tag{9}$$

Inserting $h(r) = h_0 + a - \sqrt{a^2 - r^2}$ and integrating gives the excess pressure in the slit

$$P = \left[ \frac{3}{2}\eta u_0 \frac{(h+a)H(\ln H - 1) - (h^2 + r^2 + 2ha)\ln H}{H^2 a} - 3\eta u \frac{h + a - 2H}{H^2} \right]_r^a, \tag{10}$$

where at the upper bound, the width of the cleft reads $H(a) = h + a$. The pressure vanishes for $r > a$.

Now we calculate the force exerted by the velocity field on the solid boundary. Since the normal component of the viscous stress vanishes, $\sigma_{zz}$, the force is given by the surface integral of the excess pressure,

$$F = 2\pi \int_0^R dr r P. \tag{11}$$

Notewhich gives

$$\frac{F}{6\pi\eta a} = \frac{u}{\hat{h}(1+\hat{h})}\left(1 + \frac{9}{2}\hat{h} + 3\hat{h}^2 - 3\hat{h}(1+\hat{h})^2 \ln\frac{1+\hat{h}}{\hat{h}}\right) + \frac{3}{2}u_0 \left(\frac{9}{2} + 3\hat{h} - (2 + 6\hat{h} + 3\hat{h}^2)\ln\frac{1+\hat{h}}{\hat{h}}\right). \tag{12}$$

We have replaced $h_0$ with $z$ and use the shorthand notation $\hat{h} = h/a$. Note that the slip velocity $v_0$ is related to the unconfined particle velocity $v_0 = \frac{3}{2}u_0$. The reduced velocity $u$ is determined from the condition $F = 0$, and results in

$$\frac{u}{u_0} = 3\hat{h}(1+\hat{h}) \frac{(2 + 6\hat{h} + 3\hat{h}^2)\ln\frac{\hat{h}+1}{\hat{h}} - \frac{3}{2}(3 + 2\hat{h})}{2 + 9\hat{h} + 6\hat{h}^2 - 6\hat{h}(1+\hat{h})^2 \ln\frac{\hat{h}+1}{\hat{h}}}. \tag{13}$$

The plots in the main text suggest that this expression is valid for $\hat{h} \le 0.1$. At much smaller distances, $\hat{h} \le 0.01$, power-law corrections are negligible, and we find

$$\frac{u}{u_0} = -3\hat{h}\left(\ln\hat{h} + 9/4\right) \qquad (\hat{h} \ll 1). \tag{14}$$

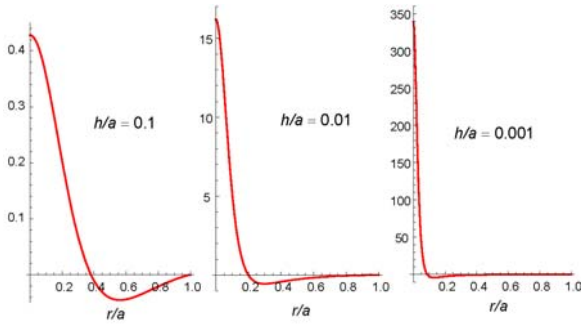


FIG. 2: Excess pressure $P(r)$ in the slit as a function of the reduced radial coordinate $r/a$ for different slit widths $h/a$.

This latter expression result from a controlled approximation in terms of the small parameter $\hat{h}$.

Reinserting the reduced velocity in (10) gives the excess pressure as a function of the unconfined particle velocity $u_0$ and the width of the slit. Fig. 2 shows $P$ as a function of the radius $r$, for different values of $h/a$, as calculated from (10) and (13). At a radial distance of roughly $2\sqrt{ha}$, the pressure changes sign. Close to the center of the slit the downward motion of the particle expels the liquid which is related to an excess pressure $P > 0$, whereas in the outer region the outward slip velocity necessitates a backflow which is accompanied by $P < 0$. The corresponding change of the sign of the radial derivative is illustrated by (9)

## II. METHOD OF REFLECTIONS

For distances larger than the particle radius, hydrodynamic interactions with the wall are treated perturbatively in terms of the method of reflections. The velocity field in the fluid is expanded in a series of fundamental solutions of Stokes' equation which are centered either at the position of the particle or at that of an image particle. The coefficients of the series are determined perturbatively in powers of $a/h$ by successive reflections of the velocity field at the particle surface and at the wall.

We start from the well-known velocity field of a freely moving particle without confinemet [5]. Chosing cylindrical coordinates and putting the origin at the solid surface, the particle is at the vertical position $z_P = a + h$ and its velocity field reads as

$$\mathbf{v}(r, z, z_P) = u_0 \frac{a^3}{R^3} \frac{3r(z - z_P)\mathbf{e}_r + [3(z - z_P)^2 - R^2]\mathbf{e}_z}{2R^2}, \tag{15}$$

where $R = \sqrt{(z_P - z)^2 - r^2}$ is the distance from the particle center. One easily verifies that $\mathbf{v}$ satisfies the slip boundary condition at the particle surface, with the effective slip velocity $\mathbf{v}_s = (1 - \mathbf{nn})\cdot\mathbf{v}|_{R=a}$, with the surface normal $\mathbf{n}$.

Usual no-slip boundary conditions require that both vertical and radial velocity components vanish at the wall. This condition is met by adding the velocity field $\hat{\mathbf{v}}$ of an image particle at $z_I = -z_P$, such that

$$(\mathbf{v} + \hat{\mathbf{v}})|_{z=0} = 0. \tag{16}$$

With the notation of Ref. [2], the image flow reads after one reflexion at the wall

$$\begin{aligned}\hat{\mathbf{v}} &= \hat{q}_3 \mathbf{v}(r, z, z_I) \\ &+u_0 \hat{p}_3 \frac{a^3}{R_I^3}\left(\frac{r}{R_I}P_3(\xi)\mathbf{e}_1 + \xi\frac{r}{R_I}\frac{P_3'(\xi)}{12}\mathbf{e}_2\right) \\ &+u_0 \hat{q}_4 \frac{a^4}{R_I^4}\left(\frac{r}{R_I}P_2(\xi)\mathbf{e}_1 + \xi\frac{r}{R_I}\frac{P_3'(\xi)}{3}\mathbf{e}_2\right). \end{aligned} \tag{17}$$

The first term is similar (15), albeit centered at the position of the image particle, $z_I = -(a+h)$, the distance from which reads $R_I = \sqrt{(z-z_I)^2 - r^2}$. Since the field $\mathbf{v} + \hat{\mathbf{v}}$ does not exactly satisfy the boundary condition on the particle surface, this solution could be improved by iterating reflexions at the particle and at the wall [2].

The remainder is given in terms of a multipole expansion with respect to the image particle We have defined the reduced vertical coordinate

$$\xi = \frac{z - z_I}{R_I}$$

and the unit vectors

$$\mathbf{e}_1 = \frac{r}{R_I}\mathbf{e}_r + \xi\mathbf{e}_z, \qquad \mathbf{e}_2 = \xi\mathbf{e}_r - \frac{r}{R_I}\mathbf{e}_z.$$

$P_n(\xi)$ are Legendre polynomials and $P_n' = \partial_\xi P_n$ their derivatives.

The coefficients $\hat{q}_3$, $\hat{p}_3$, and $\hat{q}_4$ have been determined in [2] from the boundary condition (16), and read in our notation

$$\hat{q}_3 = -\frac{11}{5}, \quad \hat{p}_3 - \frac{24}{5}, \quad \hat{q}_4 = 6\frac{h+a}{a}. \tag{18}$$

Evaluating the Legendre polynomials and their derivatives, one readily finds the radial and vertical components of $\hat{\mathbf{v}} = \hat{v}_r\mathbf{e}_r + \hat{v}_z\mathbf{e}_z$,

$$\hat{v}_r = u_0\frac{a^3}{R_I^3}\left(-15\frac{rz(z+z_P)^2}{R_I^4} + \frac{3r(3z+z_P)}{2R_I^2}\right), \tag{19}$$

$$\hat{v}_z = u_0\frac{a^3}{R_I^3}\left(15\frac{r^2z(z+z_P)}{R_I^4} + \frac{3}{2}\frac{r^2 - 4z(z+z_P)}{R_I^2} - 1\right), \tag{20}$$

which correspond to the result of Keh and Anderson [1].

The image flow field advects the particle and thus modifies its velocity. Evaluating $\hat{v}_z$ at the position $z = z_P = a + h$ and $r = 0$, we find the leading-order correction

$$u = u_0 + \hat{v}_z|_{z=z_P} = u_0\left(1 - \frac{1}{2}\frac{a^3}{(a+h)^3}\right). \tag{21}$$

The slightly different correction factor of Keh and Anderson, $\frac{5}{8}$ instead of our $\frac{1}{2}$, arises since these authors consider electrophoresis close to a perfectly conducting wall, and take the resulting deformation of the electric field into account. Similar effects would occur for thermophoresis close to a wall with infinite thermal conductivity. Since heat conduction of common materials such as PMMA and glass, is not very different from that of water, we discard the deformation of the temperature gradient due to the conductivity contrast.

## III. DEFORMATION OF THE TEMPERATURE GRADIENT

In the absence of colloidal particles, the temperature gradient $\nabla T$ is assumed to be constant, perpendicular or parallel to the capillary. A more complex field $T(\mathbf{r})$ arises in the vicinity of a colloidal particle. It satisfies Fourier's equation $\boldsymbol{\nabla}^2 T = 0$ and the usual boundary conditions at the particles-solvent and wall-solvent interfaces [2].

The change of $T(\mathbf{r})$ in the vicinity of a spherical particle and a planar wall is described by contrast factors If the

$$\alpha_n = \frac{\kappa_s - \kappa_p}{(1+\frac{1}{n})\kappa_s + \kappa_p}, \qquad \gamma = \frac{\kappa_s - \kappa_w}{\kappa_s + \kappa_w}, \tag{22}$$

which depend on the heat conductivities of the particle $\kappa_p$, the solvent $\kappa_s$, and the wall $\kappa_w$.

For a constant temperature gradient the slip velocity is $v_s^0$. (Note that $v_s^0$ is not constant along the surface but usually varies with the sine of the polar angle.) From Ref. [2] we quote the modification of the slip velocity due to the conductivity contrast. In the bulk ($h \to \infty$) one has

$$v_s^\infty = (1+\alpha_1)v_s^0 = \frac{3\kappa_s}{2\kappa_s + \kappa_p}v_s^0. \tag{23}$$

Now we consider the additional change due to the presence of the solid boundary at distance $h$. To leading order in the parameter

$$\lambda = \frac{a}{a+h}$$

one has

$$v_s = v_s^\infty\left(1 - \frac{1}{4}\frac{\alpha_1\gamma}{1+\alpha_1}\lambda^3\right). \tag{24}$$

A full derivation and higher-order corrections are found in Ref. [2]. The term $1 + \alpha_1$ does not depend on the distance $h$ and thus is of little interest here.

A distant-dependent change of the driving field arises from the remaining term, the prefactor of which reads explicitly

$$\frac{1}{4}\frac{\alpha_1\gamma}{1+\alpha_1} = \frac{1}{12}\frac{\kappa_s - \kappa_p}{\kappa_s}\frac{\kappa_s - \kappa_w}{\kappa_s + \kappa_w}.$$

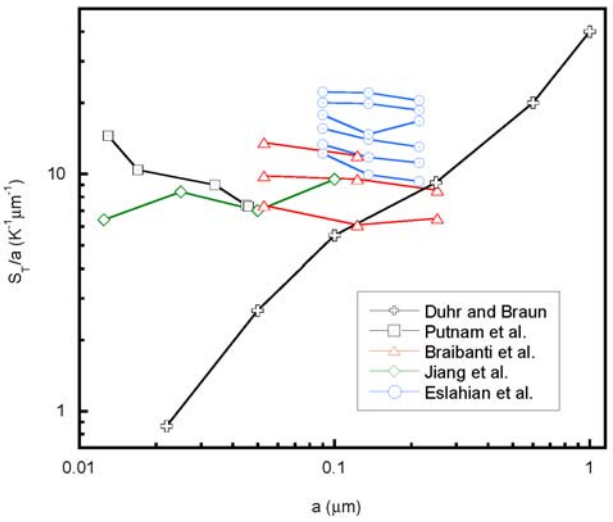


FIG. 3: Size dependence of the Soret coefficient $S_T$. For the data of five experiments on polystryene particles, the ratio of $S_T$ and the particle radius $a$ is plotted as a function of $a$. The data (+) are taken at room temperature, Duhr and Braun [11]; (□) above 35° C, Putnam et al. [7]; (△) at 25, 35, 45 °C, Braibanti et al. [8]; (◇) Jiang et al. [9]; (◯) at 28, 31, 35, 39, 44, 47 °C, Eslahian et al. [10]. The lines connect data at constant temperature.

The thermal conductivities of most relevant materials do not differ very much, and the distance-dependent contribution to the slip velocity (24) is negligible. As an example, for polystyrene beads in water close to a glass plate, the above factor takes a value of about 0.016.

Similar arguments apply to electrophoresis, where the change of the slip velocity (24) arises from the deformation of the applied electric by the permittivity contrast. Thus one has for PS particles in water ($\varepsilon_p \ll \varepsilon_s$) the factor $\alpha_1 = \frac{1}{2}$. Close to a conducting wall, Keh and Anderson calculated the distance-dependent correction to the slip velocity $v_s = v_s^\infty(1 - \frac{1}{8}\lambda^3)$ [1].

## IV. SIZE DEPENDENCE OF THE SORET COEFFICIENT

Here we complete the data given in the main text on the size dependence of the Soret coefficient. For a particle in a bulk liquid, far from the boundary, the well-known variation of the Stokes-Einstein coefficient $D_0 \propto a^{-1}$ [3] and the constant drift velocity $u_0$ =const. [4, 5], result in a linear variation $S_T^0 \propto a$.

Fig. 3 shows various Soret data for charged polystyrene particles in weak electrolyte solutions [7–11]. In these experiments the particles are at large distance from solid boundaries. In order to highlight the size dependence of the Soret coefficient, we plot the ratio $S_T/a$. The data of Putnam et al. [7], Braibanti et al. [8], Jiang et al. [9], and Eslahian et al. [10] confirm $S_T/a$ = const. as expected from theory, whereas those of Duhr and Braun [11] suggest a linear variation. Note that the data of Braibanti et al. [8] and Eslahian et al. [10] are taken at different temperatures.

TABLE I: Perpendicular thermophoresis. Soret data for polystyrene particles at room temperature. All experiments are done in capillaries, with a perpendicular temperature gradient [6, 8, 10]. Data from [8] are from Fig. 5 for 25° C; those of [10] are extrapolated to $T = 25°$ C, that of Helden et al. is taken from Fig. 4 of [6]. The values for the distance $h$ correspond to the range where data are taken [6] or to the mean value of $h$, that is, the trapping length $\ell_0 = D_0/u_0$ [10]; the numbers given for [8] give a lower bound.

| $T = 25°$ C | $S_T$ ($K^{-1}$) | $a$ ($\mu$m) | $S_T/a$ | $h$ ($\mu$m) | $h/a$ |
|---|---|---|---|---|---|
| Helden et al. [6] | 140 | 2.5 | 56 | $0.03 - 0.3$ | $0.012 - 0.12$ |
| Eslahian et al. [10] | 1.6 | 0.215 | 7.4 | 2 | 9 |
| | 1.15 | 0.136 | 8.4 | 3 | 22 |
| | 0.85 | 0.090 | 9.5 | 4.5 | 50 |
| Braibanti et al. [8] | 1.65 | 0.253 | 6.5 | $> 50$ | $> 200$ |
| | 0.75 | 0.123 | 6.0 | | |
| | 0.35 | 0.053 | 6.6 | | |

Table I gathers the data measured in a temperature gradient perpendicular to a solid boundary [6–8, 10], and Table II those where the thermal gradient is parallel to a capillary [9, 11]. Since the Soret coefficient varies significantly with temperature, we report only data taken at room temperature.Eslahian et al. [10], which cover the range from 28 to 41° C, we have extrapolated the Soret coefficient to room temperature. Regarding the data of Putnam et al. [7], it is worth noting that the large value of the smallest particle, can be related to its high surface potential: Indeed, these authors have measured the surface potential $\zeta$ of each particle; when correcting the

TABLE II: Parallel thermophoresis. Soret data for polystyrene particles at room temperature. Experiments are done in capillaries, where the temperature gradient is parallel to the boundaries [9, 11].

| $T = 25°$ C | $S_T$ ($K^{-1}$) | $a$ ($\mu$m) | $S_T/a$ | $w$ ($\mu$m) | $a/w$ |
|---|---|---|---|---|---|
| Duhr & Braun [11] | 40 | 1 | 40 | 10 | 0.1 |
| | 12 | 0.55 | 22 | | 0.055 |
| | 2.3 | 0.25 | 9.2 | | 0.025 |
| | 0.55 | 0.10 | 6.5 | | 0.010 |
| | 0.13 | 0.05 | 2.6 | | 0.005 |
| | 0.2 | 0.022 | 0.9 | | 0.0022 |
| Jiang et al. [9] | 0.95 | 0.1 | 9.5 | 2 | 0.05 |
| | 0.35 | 0.05 | 7.1 | | 0.025 |
| | 0.11 | 0.02 | 8.4 | | 0.010 |
| | 0.04 | 0.0125 | 6.5 | | 0.006 |

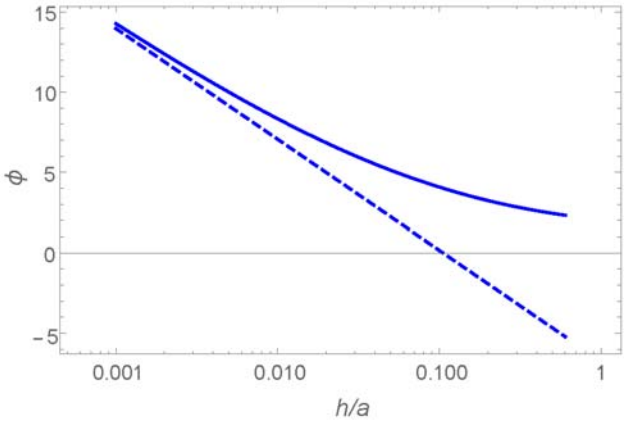


FIG. 4: Hydrodynamic boundary effects on the Soret coefficient at small distances. The solid line gives the full result obtained from lubrication approximation (25), and the dashed line from the leading-order approximation (26).

Soret coefficent for variations of $\zeta$, they find, in Fig. 7 of [7], a perfect agreement with $S_T/a = \text{const}$.

Except the measurements of Duhr and Braun, all data support the theoretical prediction $S_T/a = \text{const}$. The temperature series of Refs. [8, 10] confirm, moreover, that this law holds true at all temperatures investigated. Although surface charges and electolyte strength differ from one experiment to another, the absolute values agree rather well; the average of the nine values, $S_T^0/a = 7.4\ \text{K}^{-1}\mu\text{m}^{-1}$ is used as the bulk value in the main text.

## V. HYDRODYNAMIC BOUNDARY EFFECTS

Here we discuss boundary effects on the Soret coefficient in lubrication approximation, and the resulting probability density function for a colloidal particle close to a wall. As shown in the main text, the variation of the Soret coefficient with respect to its bulk value is expressed by $\phi = S_T/S_T^0$, with

$$\phi = 3(1+\hat{h})\frac{(2+6\hat{h}+3\hat{h}^2)\ln\frac{\hat{h}+1}{\hat{h}} - \frac{3}{2}(3+2\hat{h})}{2+9\hat{h}+6\hat{h}^2 - 6\hat{h}(1+\hat{h})^2\ln\frac{\hat{h}+1}{\hat{h}}} \qquad (25)$$

and $\hat{h} = h/a$. At very short distances, we may neglect corrections in powers of $\hat{h}$, and thus have

$$\phi = -3\left(\ln\hat{h} + \frac{9}{4}\right). \qquad (26)$$

Previous work pointed out the logarithmic law $\phi = O(\ln\hat{h})$, but did not evaluate the constants $-3$ and $-\frac{27}{4}$ [13].

In Fig. 4 we compare (25) and (26). At very short distances, $\hat{h} < 0.01$, both agree well, whereas significant differences occur for $\hat{h} > 0.01$. The leading-order expression (26) becomes negative at $\hat{h} \approx 0.1$, which is clearly unphysical, whereas the exact form is expected to be larger than unity everwhere. We conclude that the leading-order approximations, such as our Eq. (26), cease to be valid at distances larger than 0.01.

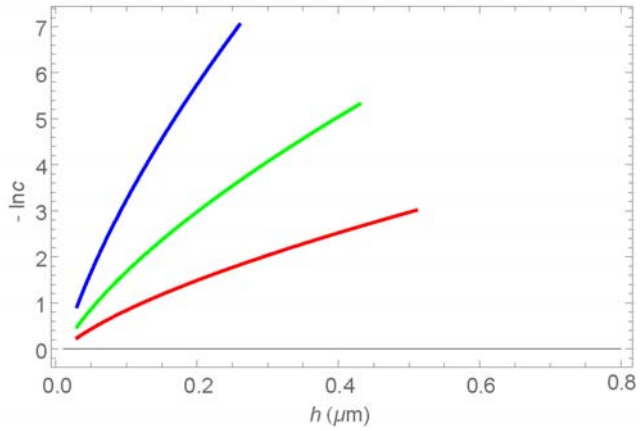


FIG. 5: Logarithm of the probability density function (28) as a function of the distance $h$, for different values of the temperature gradient. Both physical and plot parameters are chosen such that the three curves are easily compared with those of Fig. 2b of Helden et al. [6].

On the other hand, the experimentally relevant range for micron-size particles is $h/a > 0.01$. Indeed, smaller values can hardly be achieved since at distances below 10 or 20 nanometers, electric-double layer and dispersion forces overtake hydrodynamic effects. As a consequence, leading-order expressions, such (26), do not allow a meaningful comparison with experiment.

So far we have discussed corrections to the Soret coefficient $S_T$, which is proportional to the gradient of the logarithm of the probability density function,

$$-\nabla \ln c = S_T \nabla T, \qquad (27)$$

according to Eq. (1) of the main text. In Fig. 5 we plot the integral of (27), that is,

$$-\ln c(h) = S_T^0 \nabla T \Phi(h), \qquad (28)$$

with $\Phi = \int dh\phi$. The three curves are calculated for three different temperature gradients $\nabla T = 70,\ 140,\ 270$ mK/$\mu$m, which correspond to the experimental values of Fig. 2 of Helden et al. [6], and cover the same range of $h$ as the measured data. Comparison with Fig. 2b of [6] reveals a good overall agreement. The curve measured for 270 mK/$\mu$m is close to a straight line, whereas those at smaller temperature gradients are concave and rather similar to our theoretical curves. The deviations, which are strongest at very small distances $h < 100$ nm, could possibly be related to van der Waals and electric-double layer forces; at the smallest distances, however, these potential forces are significantly larger than the hydrodynamic drag.

[1] H.J. Keh, J.L. Anderson, J. Fluid Mech. **153**, 417 (1985)
[2] J. Morthomas, A. Würger, Phys. Rev. E **81**, 051405 (2010)
[3] A. Einstein, Annal. Phys. **19**, 371 (1906)
[4] N.V. Churaev, B.V. Derjaguin, V.M. Muller, *Surface Forces*, Plenum Publishing Corporation (New York 1987)
[5] J.L. Anderson, Ann. Rev. Fluid Mech. **21**, 61 (1989)
[6] L. Helden, R. Eichhorn, C. Bechinger, Soft Matter **11**, 2379 (2015)
[7] S.A. Putnam, D.G. Cahill, G.C.L. Wong, *Langmuir*, 2007 **23**, 9221.
[8] M. Braibanti, D. Vigolo, R. Piazza, Phys. Rev. Lett. **100**, 108303 (2008).
[9] H.-R. Jiang, H. Wada, N. Yoshinaga and M. Sano, *Phys. Rev. Lett.* **102**, 208301 (2009)
[10] K.A. Eslahian, A. Majee, M. Maskos, A. Würger, Soft Matter **10**, 1931 (2014)
[11] S. Duhr, D. Braun, Phys. Rev. Lett. **97**, 038103.(2006)
[12] A. Würger, Rep. Prog. Phys. **73**, 126601 (2010)
[13] T. Ishikawa, M.P. Simmonds, T.J. Pedley J. Fluid Mech. **568**, 119 (2004)